J|A|C|S COMMUNICATIONS

Published on Web 04/19/2010

Direct Observation of Nucleation and Growth in Amyloid Self-Assembly

Yan Liang,[†] David G. Lynn,*[,†] and Keith M. Berland[‡]

The Center for Fundamental and Applied Molecular Evolution and the Center for Chemical Evolution, Departments of Chemistry and Biology, Emory University, 1515 Dickey Drive, Atlanta, Georgia 30322 and Department of Physics, Emory University, 400 Dowman Drive, Atlanta, Georgia 30322

Received December 30, 2009; E-mail: dlynn2@emory.edu

The three-dimensional polypeptide ordering that occurs in protein folding is initiated within early dynamic unfolded molten globule intermediates.[1,2] While hydrophobic collapse driven backbone desolvation is critical for nucleation and assembly of native protein structure,[3] the importance of these early steps in protein misfolding and the accompanying processes that lead to amyloid-based diseases are less well understood. Early kinetic models for amyloid assembly posited that individual nucleating events create templates for the addition and conformational induction of new monomers.[4,5] Particle-like aggregates have also been detected early in assembly,[4,8] documented kinetically as on pathway,[6,7] and implicated in neuronal dysfunction.[9−12] These results have led to various nucleated conformational conversion models[13] which implicate intermediate disordered oligomer assemblies as nucleation and propagation centers.

As these general models depend on the existence, size, and composition of intermediate oligomers, we initiated fluorescence imaging and fluorescence correlation spectroscopy (FCS) experiments[14,15] to visualize the earliest events associated with intermolecular assembly. These studies required a self-assembling peptide capable of single molecule detection, and we have focused on the nucleating core of the Aβ peptide of Alzheimer's disease, Ac-KLVFFAE-NH2 (Aβ(16−22)).[16] This peptide is strongly amyloidogenic and yet forms soluble, rigid, well-characterized nanotubes,[17] which avoid fibril aggregation that so typically compromises precise characterization of nucleation and growth events with optical imaging. Replacing the lysine residue of Aβ(16−22) with Rhodamine 110 (Rh110) through solid phase synthesis generated the fluorescent monomer Rh17−22[18] which coassembles with Aβ(16−22) (Figure S1). We have employed Rh17−22 as an optical probe of the early events in amyloid assembly. Indeed, the morphologies of the mixed Rh17−22/Aβ(16−22) assemblies are indistinguishable from those obtained with pure Aβ(16−22), except that the mixed structures are homogeneously fluorescent and very bright (Figure 1A).

Circular Dichroism (CD) analyses (Figure S4) found that below a critical concentration of ∼0.5 mM, the peptides contained no assemblies and little peptide secondary structure, even after a month-long incubation. FCS measurements taken during the first few hours after the Rh17−22 peptides were mixed with different subcritical Aβ(16−22) concentrations showed that the diffusion coefficient and molecular brightness of Rh17−22 were indistinguishable from nanomolar concentrations of Rh17−22 alone (Supporting Information, Figure 1C). These measurements most likely indicate the presence of only monomeric peptides in solution (see Supporting Information), and we will refer to them as monomers throughout this manuscript. While we note that we cannot exhaustively rule out the presence of very small oligomers such as dimers or trimers of Aβ(16−22), no larger assemblies are detected. Above the critical concentration, amyloid assemblies with characteristic β secondary structure began to grow, and while extensive investigation by FCS detected no small oligomers, large, brightly fluorescent aggregates 2−8 μm in diameter appeared throughout the solution immediately after mixing (Figure 1B).

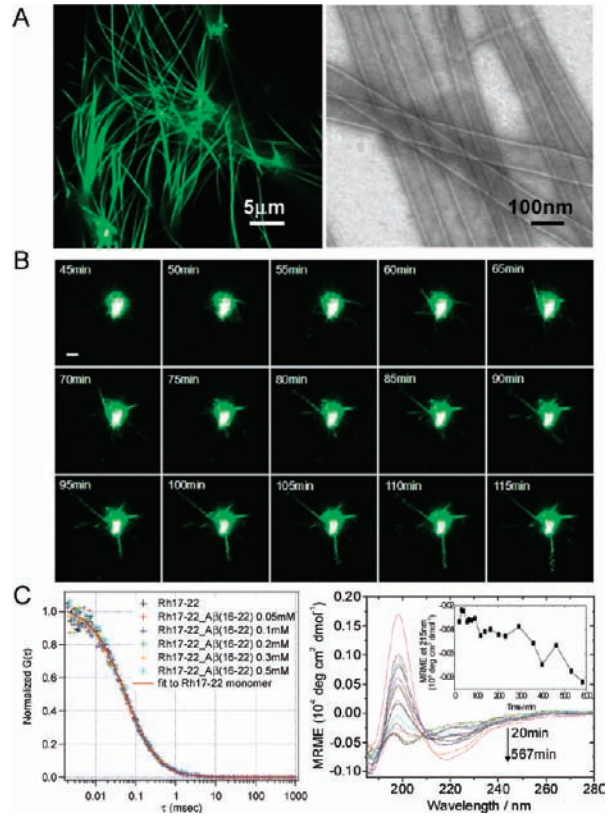

Figure 1. Aβ(16−22) assembly with Rh17−22 as probe. (A) Rh17−22 coassembled with Aβ(16−22) for 2 weeks. Left: Fluorescence imaging of 1 mM Aβ(16−22) coassembled as a 250:1 (M/M) ratio with Rh17−22. Right: The corresponding TEM image of the fluorescence tubes. (B) Time lapse fluorescence images of aggregates with emerging tubes. The images were acquired as soon as possible after Aβ(16−22) (0.6 mM) dissolved in a solution containing Rh17−22 at 4 μM (Supporting Information and Figure S6). Aggregates were apparent as soon as the peptides dissolved (∼20 min), but the tubes began appearing after 40 min. Scale = 2 μm. (C) Left: FCS of Rh17−22 (400 nM) mixed with Aβ(16−22) at the indicated concentrations. The diffusion coefficient and molecular brightness of Rh17−22 indicate that only monomeric peptide is present in solution. Right: Time-dependence of assembly taken during the first 9 h monitored by CD. The Aβ(16−22) concentration is 0.6 mM and Rh17−22/Aβ(16−22) molar ratio is 1:125. Insert: The mean residue ellipticity at 215 nm as a function of time.

[†] The Center for Fundamental and Applied Molecular Evolution and the Center for Chemical Evolution, Departments of Chemistry and Biology.
[‡] Department of Physics.

10.1021/ja910964c

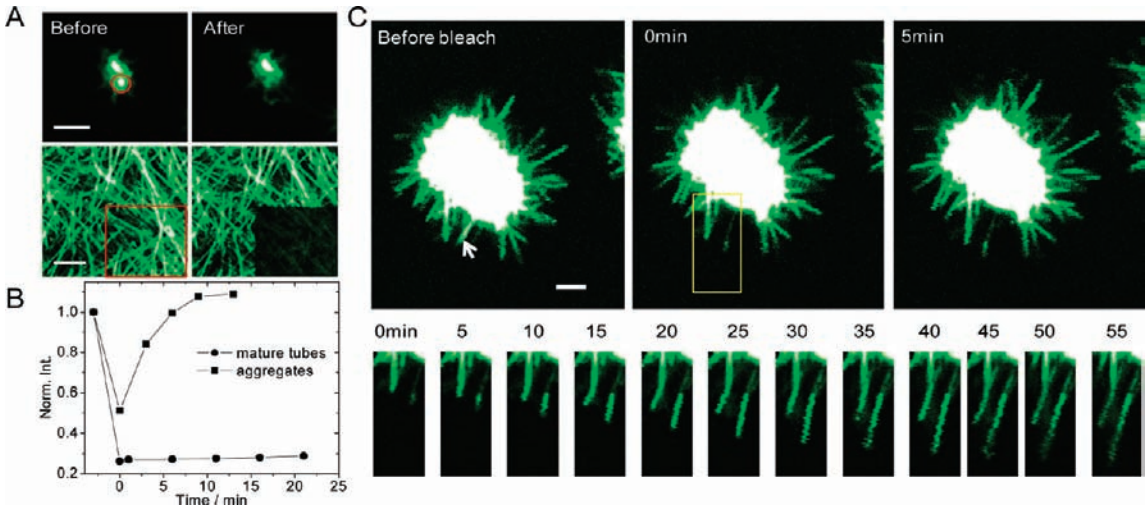

Figure 2. Peptide motions within aggregates and mature assemblies. Aβ(16−22)/Rh17−22 (0.6 mM/4 μM) aggregates were imaged in a 5 μL volume (A) Before and After photobleaching of aggregates (top) and mature assemblies (bottom) with the bleached region indicated by the red circle and square, respectively. Scale=5 μm. (B) Recovery of the integrated fluorescence intensity measured in 3−5 min intervals from the indicated regions in (A). (C) The elongating amyloids were photobleached within the yellow square and the growing end indicated by the white arrow was followed in time. Panels below represent fluorescence images recorded over an hour at 5 min intervals. The amyloid continues to elongate, but the photobleached region does not change position relative to the aggregate, indicating that elongation proceeds dominantly if not exclusively from the amyloid ends.

For a sample prepared just above the critical concentration, we estimate that during the first few hours postmixing roughly half of the initial peptide concentration was sequestered within the aggregates. Like the FCS measurements at subcritical Aβ(16−22) concentrations, FCS measurements performed in solution near the aggregates detected only monomeric Rh17−22 peptide (Table S1, Figure S3), both during the early postmixing hours and after mature amyloid structure had developed.

While some amyloidogenic peptides are surface active,[19] these assemblies are much too large for micelles composed of such short peptides, and indeed no evidence could be found for aggregate formation at air/water interfaces, a critical stage in micelle/vesicle assembly.[20] And quite unlike micelle/vesicle organization, optical dissection found the aggregates to be homogeneously fluorescent throughout their interior. The assemblies then appear to emerge by phase separation throughout the solution.

To better define the nature of these aggregates, peptide site exchange was monitored within the aggregates via fluorescence recovery following a photobleaching pulse (Figure 2A). Relative to the mature assemblies where the peptides are hydrogen bonded within β-sheets and no significant recovery occurs (Figure 2A), the time course of fluorescence recovery in the aggregate is rapid and complete within minutes (Figure 2B). Relative to the diffusion of the fluorescence peptide monomers in solution (Table S1), the

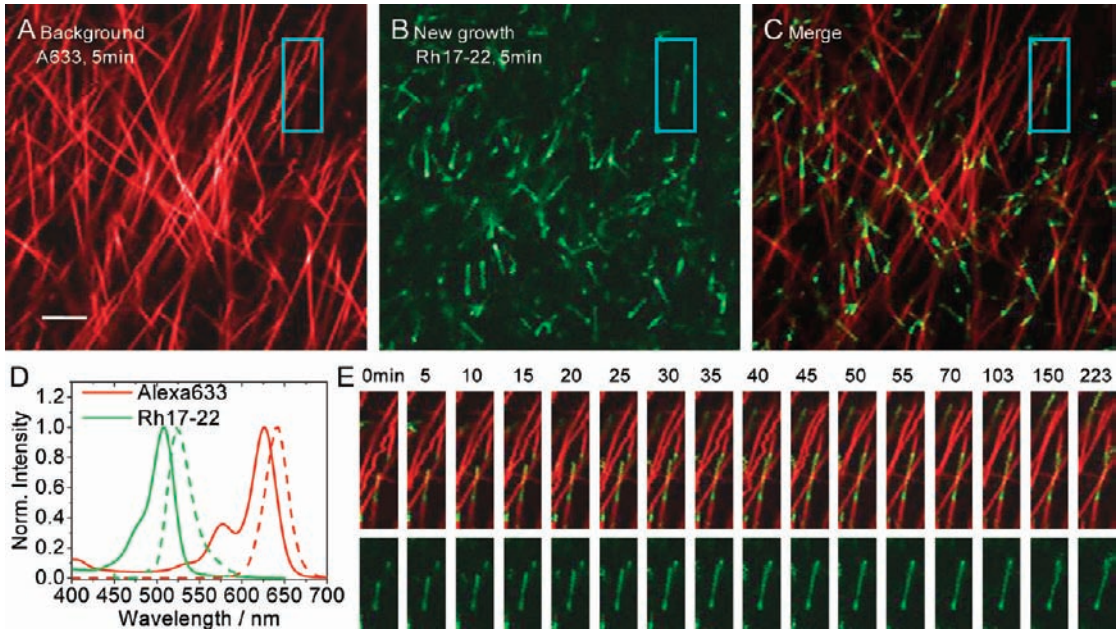

Figure 3. Mature amyloids dynamically assemble at the ends. Contrast is achieved with Alexa 633 which binds mature Aβ(16−22) (1 mM) assemblies and Rh17−22, which is specifically incorporated in new growth and does not interact with mature amyloid. (A) Mature Aβ(16−22) assemblies highlighted with Alexa 633 5 min after adding Rh17−22. (B) The corresponding image of Rh17−22, showing regions of new growth. (C) The overlay of A and B with Alexa 633 (red) and Rh17−22 (green). Scale = 5 μm. (D) Absorbance and emission spectra of Alexa 633 and Rh110 show minimal spectral overlap of the fluorescence emission. (E) Time course over 3 h of the regions highlighted by the cyan square in (A)−(C).

recovery rate in the aggregates indicates dense packing, but with few if any rigidifying intermolecular associations[17] characteristic of amyloid secondary structure. The peptide dynamics within the aggregates are similar to the intramolecular molten globule assemblies seen during protein folding,[21] but these assemblies arise from intermolecular aggregation (Figure 1C).

The most striking feature is seen in the time-lapsed images where the amyloid assemblies (Figure 1B) emerge exclusively from within the aggregates (see movie, Supporting Information). These images suggest that the larger the aggregate, the greater the number of amyloid assemblies that emerge, consistent with the difficulty of detecting nucleation within the smaller particles of other amyloid assemblies. As the assemblies mature, the large aggregates diminish to leave the mature amyloid in solution (Supporting Information). The estimated density of the aggregates, based on the FCS and fluorescence intensity measurements, approaches that of folded proteins. Therefore, the aggregates are densely packed, are likely driven by hydrophobic collapse, and assume a desolvated state that is critical for amyloid nucleation.[22]

To test whether propagation also occurs within the aggregate, time lapsed images of the growing ends of the emerging amyloid were recorded following photobleaching (Figure 2C). These amyloid ends continue to elongate, but the photobleached area maintains its position relative to the aggregate (Figure 2C). Therefore, even with the high density of peptides within the aggregate, growth occurs in solution. FCS measurements near these propagating ends (Figure S3 and Table S1) detected no oligomeric assemblies, establishing that peptide monomers contribute to propagation. When the measured growth rate of 0.15 μm/min (Figure 2C), consistent with previous measurements of amyloid propagation,[23] is combined with the known final structure of the assembly, a net addition of 2000 peptides occur every second under these conditions.

The photobleaching experiments in Figure 2 establish that peptides in the mature assemblies exchange only slowly. To test whether the active ends remain in dynamic equilibrium with bulk solution (Figure S5), the mature amyloid was stained with Alexa 633 (Figure 3A), a fluorescent dye that intensely stains the tubes when added to already mature structures and has little spectral overlap with Rh17−22 (Figure 3D). In contrast to Alexa 633, Rh17−22 added to the sample does not stain pre-existing amyloid structures but can be incorporated into a newly assembled amyloid. New growth can thus be clearly visualized by adding Rh17−22 (2 μM) to the sample (Figure 3A−C). New growth was clearly visualized within a few minutes using synchronized two-channel imaging at 530 nm and 645 nm (Figure 3E), consistent with the generally accepted amyloid-seeded growth initiated by prenucleated structures.[24] Such a dynamic system is critical for transmission and infection in prion[25,26] and possibly other amyloid diseases.

These results establish that protein folding and misfolding may differ only subtly in the multiplicity of the earliest molten intermediates. The size of the protein appears inversely related to this aggregate multiplicity, and the small nucleating center of Aβ is fortuitous in making large particles where the probability for nucleation is high and easily observed. Current lattice models of similarly small amyloidogenic peptides have now captured many features of the nucleated growth, templated assembly, and nucleated conformational conversion models,[27] and these new experimental constraints extend these models. And maybe most importantly, the realization that initiation likely occurs within an intermolecular molten globule explains the strong dependence on hydrophobic character in amyloid propensity[28−30] and argues that these early assemblies must be opportune sites for therapeutic intervention. The dependence on such intermolecular aggregates may also involve multiple proteins, recasting the long-standing issue of tissue specificity as an environment that facilitates nucleation of a toxic amyloid.[31]

Acknowledgment. This work was funded by the U.S. DOE (ER15377), NSF-CRC-CHE-0404677, NSF-CBC-0739189, and NSF MCB-0817966.

Supporting Information Available: Synthetic and experimental details. This material is available free of charge via the Internet at http://pubs.acs.org.

References

(1) Pace, C. N.; Shirley, B. A.; Mcnutt, M.; Gajiwala, K. *FASEB J.* **1996**, *10*, 75–83.
(2) Dinner, A. R.; Sali, A.; Smith, L. J.; Dobson, C. M.; Karplus, M. *Trends Biochem. Sci.* **2000**, *25*, 331–339.
(3) Rose, G. D.; Fleming, P. J.; Banavar, J. R.; Maritan, A. *Proc. Natl. Acad. Sci. U.S.A.* **2006**, *103*, 16623–16633.
(4) Harper, J. D.; Peter, T.; Lansbury, J. *Annu. Rev. Biochem.* **1997**, *66*, 385–407.
(5) Uversky, V. N.; Fink, A. L. *Biochim. Biophys. Acta* **2004**, *1698*, 131–153.
(6) Morinagaa, A; Hasegawaa, K; Nomuraa, R; Ookoshia, T; Ozawaa, D; Gotoc, Y; Yamadab M; Naiki, H. *Biochem. Biophys. Acta* **2010**, doi: 10.1016/j.bbapap.2010.01.012.
(7) Hellstrand, E.; Boland, B.; Walsh, D. M.; Linse, S. *ACS Chem. Neurosci.* **2010**, *1*, 13–18.
(8) Stine, W. B.; Dahlgren, K. N.; Krafft, G. A.; LaDu, M. J. *J. Biol. Chem.* **2003**, *278*, 11612–11622.
(9) Walsh, D. M.; Selkoe, D. J. *J. Neurochem.* **2007**, *101*, 1172–1184.
(10) Gosal, W. S.; Morten, I. J.; Hewitt, E. W.; Smith, D. A.; Thomson, N. H.; Radford, S. E. *J. Mol. Biol.* **2005**, *351*, 850–864.
(11) Necula, M.; Kayed, R.; Milton, S.; Glabe, C. G. *J. Biol. Chem.* **2007**, *282*, 10311–10324.
(12) Kayed, R.; Head, E.; Thompson, J. L.; McIntire, T. M.; Milton, S. C.; Cotman, C. W.; Glabe, C. G. *Science* **2003**, *300*, 486–489.
(13) Serio, T. R.; Cashikar, A. G.; Kowal, A. S.; Sawicki, G. J.; Moslehi, J. J.; Serpell, L.; Arnsdorf, M. F.; Lindquist, S. L. *Science* **2000**, *289*, 1317–1321.
(14) Rigler, R.; Elson, E. *Fluorescence Correlation Spectroscopy: Theory and Applications*; Springer: New York, 2001.
(15) Chen, Y.; Muller, J. D.; So, P. T. C.; Gratton, E. *Biophys. J.* **1999**, *77*, 553–567.
(16) Lu, K.; Jacob, J.; Thiyagarajan, P.; Conticello, V. P.; Lynn, D. G. *J. Am. Chem. Soc.* **2003**, *125*, 6391–6393.
(17) Mehta, A. K.; Lu, K.; Childers, W. S.; Liang, Y.; Dublin, S. N.; Dong, J.; Snyder, J. P.; Pingali, S. V.; Thiyagarajan, P.; Lynn, D. G. *J. Am. Chem. Soc.* **2008**, *130*, 9829–9835.
(18) Liang, Y.; Guo, P.; Pingali, S. V.; Pabit, S.; Thiyagarajan, P.; Berland, K. M.; Lynn, D. G. *Chem. Commun.* **2008**, *48*, 6522–6524.
(19) Ambroggio, E. E.; Kim, D. H.; Separovic, F.; Barrow, C. J.; Barnham, K. J.; Bagatolli, L. A.; Fidelio, G. D. *Biophys. J.* **2005**, *88*, 2706–2713.
(20) Chari, K.; Seo, Y.-S.; Satija, S. *J. Phys. Chem. B* **2004**, *108*, 11442–11446.
(21) Dobson, C. M. *Curr. Biol.* **1994**, *4*, 636–640.
(22) Liang, Y.; Pingali, S. V.; Jogalekar, A. S.; Snyder, J. P.; Thiyagarajan, P.; Lynn, D. G. *Biochemistry* **2008**, *47*, 10018–10026.
(23) Yagi, H.; Ban, T.; Morigaki, K.; Naiki, H.; Goto, Y. *Biochemistry* **2007**, *46*, 15009–15017.
(24) Colby, D. W.; Zhang, Q.; Wang, S.; Groth, D.; Legname, G.; Riesner, D.; Prusiner, S. B. *Proc. Natl. Acad. Sci. U.S.A.* **2007**, *104*, 20914–20919.
(25) Porcher, E.; Gatto, A. *J. Theor. Biol.* **2000**, *205*, 283–296.
(26) Linden, R.; Martins, V. R.; Prado, M. A. M.; Cammarota, M.; Izquierdo, I.; Brentani, R. R. *Physiol. Rev.* **2008**, *88*, 673–728.
(27) Chen, J.; Bryngelson, J. D.; Thirumalai, D. *J. Phys. Chem. B* **2008**, *112*, 16115–16120.
(28) Chiti, F.; Stefani, M.; Taddei, N.; Ramponi, G.; Dobson, C. M. *Nature* **2003**, *424*, 805–808.
(29) Valerio, M.; Colosimo, A.; Conti, F.; Giuliani, A.; Grottesi, A.; Manetti, C.; Zbilut, a. J. P. *Proteins: Struct., Funct., Bioinform.* **2005**, *58*, 110–118.
(30) Meijer, J. T.; Roeters, M.; Viola, V.; Lowik, D. W. P. M.; Vriend, G.; Hest, J. C. M. v. *Langmuir* **2007**, *23*, 2058–2063.
(31) Pahnke, J.; Walker, L. C.; Scheffler, K.; Krohn, M. *Neurosci. Biobehav. Rev.* **2009**, *33*, 1099–1108.

JA910964C